

LETTER • **OPEN ACCESS**

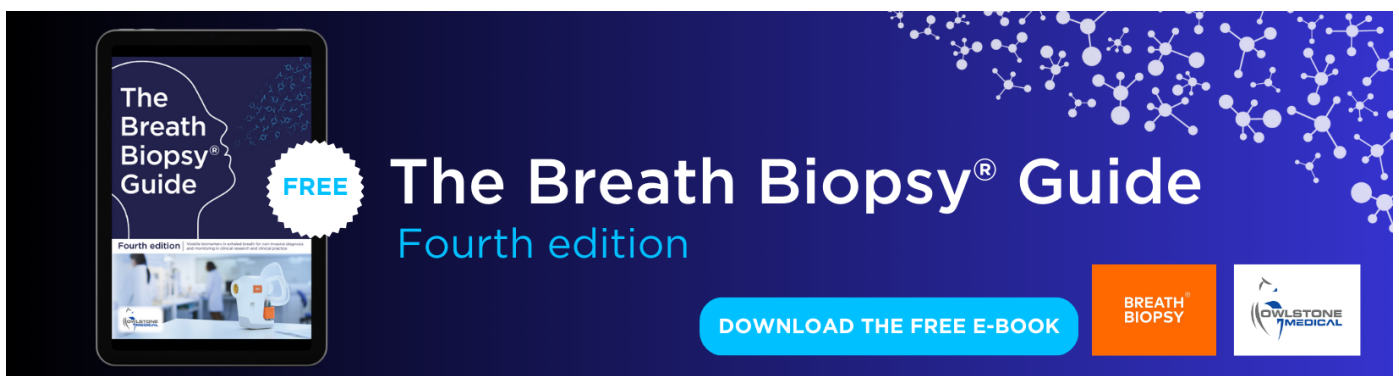
Shutdown of Atlantic overturning circulation could cause persistent increase of primary production in the Pacific

To cite this article: Ralf Liebermann *et al* 2024 *Environ. Res. Lett.* **19** 024005

View the [article online](#) for updates and enhancements.

You may also like

- [Impact of the GeoMIP G1 sunshade geoengineering experiment on the Atlantic meridional overturning circulation](#)
Yu Hong, John C Moore, Svetlana Jevrejeva *et al.*
- [Modeling evidence for large, ENSO-driven interannual wintertime AMOC variability](#)
K L Smith and L M Polvani
- [Reply to Comment on 'On the relationship between Atlantic meridional overturning circulation slowdown and global surface warming'](#)
L Caesar, S Rahmstorf and G Feulner



The Breath Biopsy® Guide
Fourth edition

FREE

DOWNLOAD THE FREE E-BOOK

BREATH BIOPSY

OWLSTONE MEDICAL

ENVIRONMENTAL RESEARCH
LETTERS

LETTER

Shutdown of Atlantic overturning circulation could cause persistent increase of primary production in the Pacific

OPEN ACCESS

RECEIVED
31 August 2023REVISED
4 December 2023ACCEPTED FOR PUBLICATION
20 December 2023PUBLISHED
18 January 2024

Original Content from
this work may be used
under the terms of the
[Creative Commons
Attribution 4.0 licence](#).

Any further distribution
of this work must
maintain attribution to
the author(s) and the title
of the work, journal
citation and DOI.



Ralf Liebermann* , Matthias Hofmann and Georg Feulner

Earth System Analysis, Potsdam Institute for Climate Impact Research, Member of the Leibniz Association, Potsdam, Germany
* Author to whom any correspondence should be addressed.E-mail: liebermann@pik-potsdam.de**Keywords:** climate change, ocean biogeochemistry, tipping elements, Atlantic meridional overturning circulation, Pacific, North Atlantic, HNLCSupplementary material for this article is available [online](#)

Abstract

A potential shutdown of the Atlantic meridional overturning circulation (AMOC) is commonly recognized to have a significant impact on the Northern hemispheric climate, notably in Northern Europe. The collapse of the northbound heat transport by the AMOC is supposed to cool down surface air temperatures at the Scandinavian coast by up to 6 K accompanied by a concomitant nutrient starvation of phytoplankton in Subarctic and Arctic regions. However, besides local and regional impacts, tipping the AMOC into a weaker state by anthropogenic carbon dioxide (CO₂) and associated freshwater forcing could also have surprising remote effects. In order to investigate possible long-term impacts of an AMOC shutdown on ocean biogeochemistry, we employ an Earth system model of intermediate complexity using idealized scenarios of century-scale atmospheric 2×CO₂ and 4×CO₂ pulses combined with North Atlantic freshwater forcing. The results show a continued increase in primary production, in particular in the Eastern equatorial Pacific, due to a decrease in iron limitation following the AMOC shutdown. Tracer simulations indicate that bioavailable dissolved iron brought by Aeolian dust into the subtropical gyres of the Atlantic Ocean is transported to the Southern Ocean and from there enters the Indian Ocean and the Pacific. Thereby, the additionally introduced iron fertilizes the phosphate-rich high-nutrient, low chlorophyll waters, giving a lasting boost to phytoplankton growth, especially in the Eastern equatorial Pacific.

1. Introduction

Phytoplankton forms the base of the marine food web and is an integral component of the global carbon cycle. The current global distribution of pelagic biological production zones reveals a typical spatial pattern which can be characterized by four biomes (polar, westerlies, trade winds, tropical; Vichi *et al* 2011) and their subdivision into 56 ocean biogeochemical provinces (Longhurst *et al* 1995, Reygondeau *et al* 2013, 2020). In this context, the Southern Ocean (SO), the Western subarctic Pacific and the equatorial Pacific are regarded as the most prominent high nutrient, low chlorophyll (HNLC) provinces in the global ocean. These areas are characterized by a comparatively low biological productivity despite a sufficiently high abundance of macro-nutrients such as

nitrate (NO₃⁻) and phosphate (PO₄³⁻). Furthermore, HNLC areas also exhibit low concentrations of micro-nutrients where the most important constituent is bioavailable iron. Already during the late eighties of the previous century, Martin and Fitzwater (1988) proposed iron limitation as the most probable cause of the existence of HNLC areas.

In their seminal papers, Kolber *et al* (1994) and Behrenfeld *et al* (1996) identified the Eastern equatorial Pacific (EEP) as a region of pronounced iron limitation with respect to phytoplankton photosynthesis and primary production. *In situ* iron enrichment experiments (IronEx II, Landry *et al* 2000) caused a relaxation of iron limitation in several spots in the EEP lasting over a couple of weeks by provoking a large increase in phytoplankton biomass and a shift in the community size structure towards larger cells,

notably diatoms. Therefore, the results from IronEx II are regarded as a confirmation of the iron limitation hypothesis for the EEP HNLC province.

Current climatological estimates of annual net primary production (NPP) in the EEP range between about 4.5 and 6.5 gigatons of carbon per year (Rousseaux *et al* 2014; GtC yr^{-1} , $1\text{Gt} = 10^{15}\text{g}$), which is about 10% the total global ocean NPP based on a value of 50 GtC yr^{-1} derived from remote sensing data (Field *et al* 1998). The Southern Ocean (SO), a second important HNLC zone, contributes a comparable amount of NPP of the order of 5 GtC yr^{-1} .

Recent climate projections utilizing a variety of anthropogenic greenhouse gas emission scenarios by employing a suite of CMIP5/CMIP6-type models reveal an overall weakening of NPP on the global scale (Kwiatkowski *et al* 2020, Reygondeau *et al* 2020). As global mean sea surface temperatures (SSTs) rise, upper oceans stratification strengthens with the consequence of a steepening of the nutricline. As a result, less nutrients from the sub-surface layer will replenish the water masses in the euphotic zone. In this context the equatorial Pacific production zone is projected to shrink by the year 2100 under RCP-2.6 and RCP-8.5 emission scenarios (Reygondeau *et al* 2020).

In order to get deeper insights into the stability of the Earth's climate system under anthropogenic forcing, it is of greatest interest to identify and pinpoint potential tipping elements (Lenton *et al* 2008, Steffen *et al* 2021). Besides utilization of socio-economically based emission scenarios, it is often useful to artificially disturb an Earth system model by applying a pulse-like external forcing and to analyze the subsequent climate response. A classical example is freshwater hosing of the North Atlantic (NA) to provoke a shutdown of the Atlantic meridional overturning circulation (AMOC; Rahmstorf 1995, Liu *et al* 2017). This is particularly relevant in light of increased meltwater input from the Greenland ice sheet expected under future warming (Caesar *et al* 2018, Hofer *et al* 2020, Weijer *et al* 2020).

Starting from a preindustrial $p\text{CO}_2$ value of 280 ppmv, typical idealized experimental set-ups utilize prescribed exponentially growing atmospheric carbon dioxide (CO_2) levels up to a certain limit (e.g. $2\times\text{CO}_2$, $4\times\text{CO}_2$) followed by a subsequent transient decline to its initial level to trigger climate system responses capable to force the whole system into a new state (Jeltsch-Thoemmes *et al* 2020). This kind of experiments can be regarded as an attempt to probe the existence of potential tipping points (Lenton *et al* 2008) in an Earth system model.

Here we apply a comparable atmospheric CO_2 forcing to an Earth system model of intermediate complexity (EMIC), and combine it with a concomitant freshwater flux anomaly in the NA. As a result, in the aftermath of the perturbation when atmospheric CO_2 reaches its preindustrial level again, NPP in the

EEP increases on century scale by up to 10 per cent. In this context, we are investigating whether a prolonged weakening or shutdown of the AMOC could cause an increase in NPP in the Pacific due to enhanced near-surface transport of bioavailable iron from the Atlantic.

2. Methods

2.1. Model

CLIMBER-3 α +C (Montoya *et al* 2005, Mathesius *et al* 2015, Hofmann *et al* 2019) is an EMIC and stays in line with the CMIP5/CMIP6-simulations (Séférian *et al* 2020). It comprises a revamped version of the ocean general circulation model (OGCM) MOM-3 (Pacanowski and Griffies 1999, Hofmann and Morales Maqueda 2006) including a marine carbon cycle model (see below), the dynamic/thermodynamic sea ice model ISIS (Fichefet and Morales Maqueda 1997), and a statistical-dynamical model of the atmosphere (POTSDAM-2, Petoukhov *et al* 2000) whereby an assumption of a universal vertical structure is made. Emission, atmospheric transport and deposition of Aeolian dust (which provides a source for bio-available iron to the ocean) is implemented according to Bauer and Ganopolski (2010). The spatio-temporal distribution of terrestrial vegetation types and inland ice is described according to climatological data sets (Montoya *et al* 2005). The horizontal resolution of the ocean component of $3.75^\circ\times 3.75^\circ$ is rather coarse but finer than that of the atmosphere ($7.5^\circ\times 22.5^\circ$). Vertically, the ocean is divided into 24 layers with thickness increasing from 25 m for the uppermost layer to about 500 m for the lowest layer.

2.2. Marine carbon cycle and biogeochemistry

An interactively coupled marine carbon cycle and biogeochemistry model operates in CLIMBER-3 α +C which exchanges fluxes and tracer concentrations with the OGCM MOM-3 and provides CO_2 levels to the long wave radiation module of POTSDAM-2. Its development branches off from the Hamburg ocean carbon cycle model version 3.1 (HAMOCC-3.1, Six and Maier-Reimer 1996) and includes several upgrades such as a simple parameterization of the marine iron cycle (Parekh *et al* 2005) and a mineral ballast driven vertical export of biogenic matter (Hofmann and Schellnhuber 2009, Hofmann *et al* 2019). The OGCM MOM-3 employs an interactive and circulation dependent parameterization of the transport of mesoscale eddies (Hofmann and Morales Maqueda 2011).

The marine ecosystem submodel follows the 'nutrient, phytoplankton, zooplankton, detritus' (NPZD) concept (Fasham 1993) and assumes a fixed Redfield stoichiometry between carbon, nitrate, phosphate, oxygen, and iron $\text{C:P:N:O:Fe} = 122:16:1:(-172):0.5\times 10^{-3}$ (Six and Maier-Reimer

1996). Besides the dynamics of inorganic ocean tracers such as dissolved inorganic carbon (DIC), alkalinity (ALKA), phosphate (PO_4^{3-}), oxygen (O_2), silicate (SiO_4^{4-}), and total dissolved iron (Fe_T) the model also accounts for the living matter (phytoplankton, zooplankton) and their products detritus, dissolved organic carbon (DOC), and calcite shells (CaCO_3).

The terrestrial carbon cycle coupled to CLIMBER-3 α +C was parameterized by employing a simple box model (Hofmann *et al* 2019) akin to MAGICC (Meinshausen *et al* 2011) comprising a plant, a litter, and a soil carbon box. However, the model does not account for land-use change.

2.3. Iron co-limitation

For the sake of simplicity and computational performance, CLIMBER-3 α +C only simulates the dynamics of one single macro-nutrient: phosphate (PO_4^{3-}). Phosphate limitation of phytoplankton growth is parameterized along a Michaelis–Menten term

$$L_{\text{PO}_4} = \frac{[\text{PO}_4^{-3}]}{[\text{PO}_4^{-3}] + P_0}, \quad (1)$$

where $P_0 = 0.008 \mu\text{mol l}^{-1}$ is the half saturation constant and $[\text{PO}_4^{-3}]$ the phosphate ion concentration computed by CLIMBER-3 α +C.

Besides the macro-nutrient phosphate, the model also accounts for the kinetics of the micro-nutrient iron. The iron limitation factor L_{Fe} of phytoplankton growth is also parameterized according to a Michaelis–Menten function

$$L_{\text{Fe}} = \frac{[\text{Fe}_T]}{[\text{Fe}_T] + F(\text{SST})}. \quad (2)$$

Here, $[\text{Fe}_T]$ – the total dissolved iron concentration, which is calculated according to Parekh *et al* (2005)—is in units of $\mu\text{mol l}^{-1}$ and the half saturation constant is assumed to be a function depending on SST in $^\circ\text{C}$:

$$F(\text{SST}) = \max(8.0 \times 10^{-5}, f(\text{SST}))$$

with

$$f(\text{SST}) = 10^{-3} \times \frac{T_{\text{Fe}1} - \text{SST}}{T_{\text{Fe}1} - \text{SST} + T_{\text{Fe}2}},$$

which serves as an empirical allometric correction factor (EACF), where $T_{\text{Fe}1} = 32 \text{ }^\circ\text{C}$ and $T_{\text{Fe}2} = 60 \text{ }^\circ\text{C}$ are simple tuning parameters which provide almost realistic spatial Fe_T distribution pattern in CLIMBER-3 α +C (see figure S3). The EACF accounts for the different iron demand of different phytoplankton cell sizes. While smaller species with a higher surface to volume ratio and dwelling in warm tropical waters have a lower demand on bioavailable iron, larger cells

living in cold polar regions need higher iron concentrations to grow (Sunda and Huntsman 1997).

Due to the general nutrient deficiency of the photic zone, a depth of 100 m was chosen for the geographical analysis, as this is where the assumed nutrient limitation can best be read.

2.4. External climate forcing and emission scenarios

Application of climate forcings have been started after a spin-up of several thousand simulation years at atmospheric CO_2 concentrations of 280 ppm (baseline), so that the simulated Earth system state could stabilize first under conditions similar to the pre-industrial era. Then six different scenarios were explored in separate runs, combining CO_2 and freshwater forcing (see figures 1(a) and (b), which are:

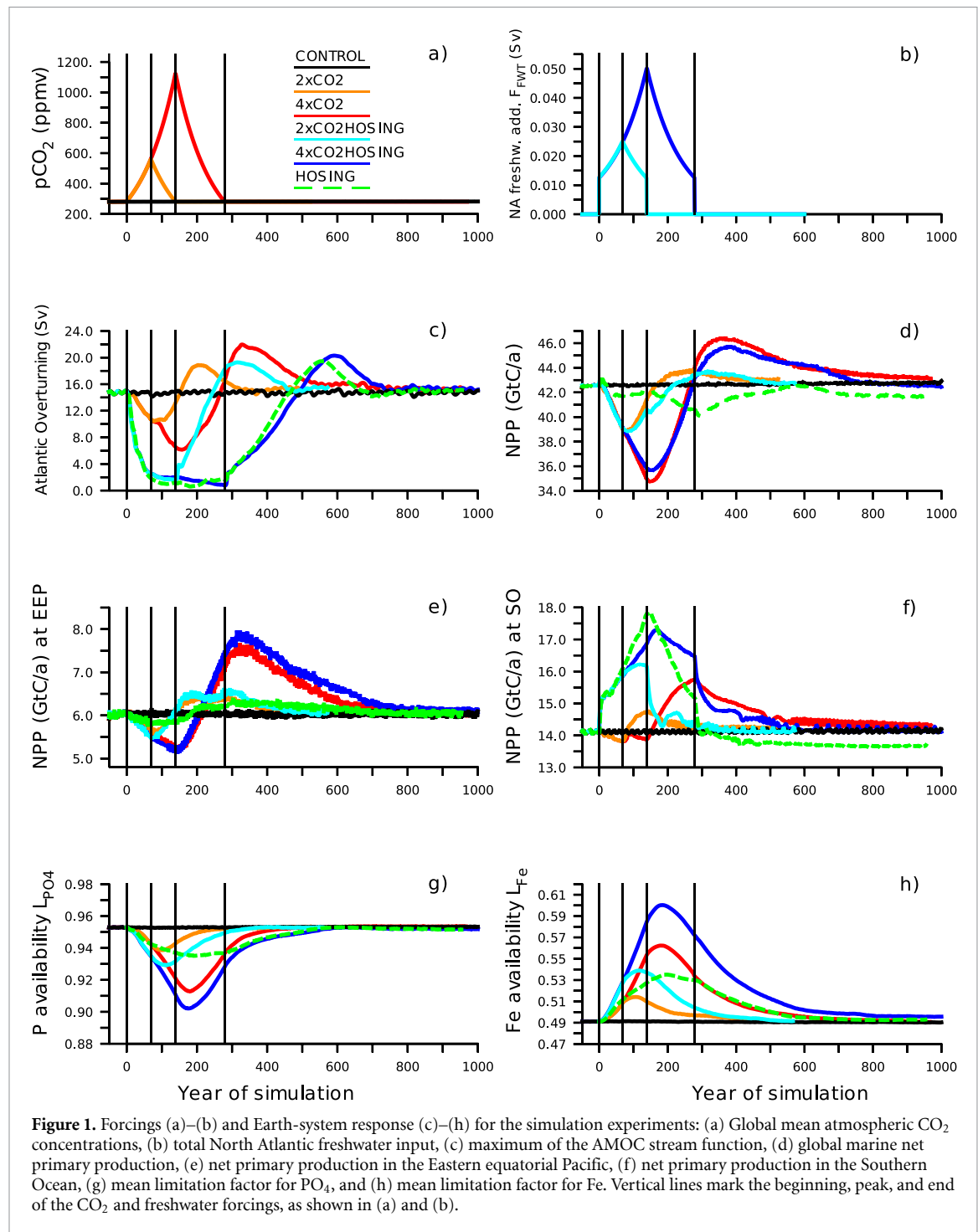
- (i) CONTROL: control run with CO_2 remaining at pre-industrial levels, i.e. baseline, with no freshwater addition. In this scenario, the model shows a drift per century of -1 GtC for total CO_2 , 0.05 GtC for NPP and 0.2 ppm for pCO_2 . Maximum AMOC strength shows no drift but oscillates around $14.5 \pm 0.5 \text{ Sv}$.
- (ii) $2 \times \text{CO}_2$: 1 % increase of atmospheric CO_2 concentrations until a doubling is reached, declining symmetrically afterwards back to baseline.
- (iii) $4 \times \text{CO}_2$: similar to $2 \times \text{CO}_2$ but peaking at fourfold baseline CO_2 levels.
- (iv) $2 \times \text{CO}_2$ HOSING: same as $2 \times \text{CO}_2$ except for additional NA freshwater forcing of $F_{\text{FWT}} \leq 0.025 \text{ Sv}$ uniformly distributed between 55°N and 75°N commencing 50 years after CO_2 increase.
- (v) $4 \times \text{CO}_2$ HOSING: same as $4 \times \text{CO}_2$ except for additional NA freshwater forcing of $F_{\text{FWT}} \leq 0.05 \text{ Sv}$.
- (vi) HOSING: same NA freshwater forcing of $F_{\text{FWT}} \leq 0.05 \text{ Sv}$ as in $4 \times \text{CO}_2$ scenario but without CO_2 increase.

The idealized freshwater hosing scenarios emulate the effects of Greenland meltwater input into the NA in CLIMBER-3 α +C, which cannot simulate dynamic melting of ice sheets. Values for freshwater forcing of $F_{\text{FWT}} \leq 0.05 \text{ Sv}$ ($1 \text{ Sv} = 10^6 \text{ m}^3 \text{ s}^{-1}$) are in line with recent CMIP6 simulations under the SSP585 emission path revealing a surface mass balance anomaly of the Greenland ice sheet of -1332 Gt yr^{-1} (0.042 Sv) by the end of the 21st century (Hofer *et al* 2020).

3. Results

3.1. AMOC weakening

As can be seen in figure 1(c), the AMOC stream function decreases in all simulation experiments, followed by a recovery above the baseline level,



whereby the extent and duration depend largely on the respective scenario. Thus, the simulations without fresh water input (2×CO₂ and 4×CO₂) show a reduction of about 30% and 60%, respectively, after which a recovery occurs immediately and the AMOC returns to the baseline level at the end of the CO₂ forcing. In the scenarios with freshwater input into the NA (HOSING, 2×CO₂HOSING, and 4×CO₂HOSING), on the other hand, there is a decrease in AMOC strength of about 90%, which corresponds to a total shutdown. The subsequent recovery phase seems to depend exclusively on the amount

of freshwater supplied: in the case of HOSING and 4×CO₂HOSING, recovery to the base level occurs approximately at $T = 500$, more than 200 years after the end of the forcings and the recovery for scenario 2×CO₂HOSING.

3.2. Transient and long-term NPP changes

For all scenarios, a long-term increase of global NPP was found, following a transient decrease during the period of elevated CO₂ (see figure 1(d)). The strongest NPP decrease always occurs a few years after reaching the CO₂ maximum of the

respective scenario. A maximum NPP decrease of 15%–20% is shown for $4\times\text{CO}_2$ and $4\times\text{CO}_2\text{HOSING}$, while the NPP for the ‘weaker’ scenarios $2\times\text{CO}_2$ and $2\times\text{CO}_2\text{HOSING}$ decrease by less than 10%. Subsequently, the global NPP recovers rapidly, whereby the minimum AMOC strength and the maximum recovery rate for NPP coincide for $4\times\text{CO}_2\text{HOSING}$, and rises above the baseline value to reach its maximum about 100 years (depending on the scenario) after the return to the pre-industrial CO_2 level. As with the preceding decrease, the maximum NPP increase is by far the strongest in scenarios $4\times\text{CO}_2$ (ca. 10%) and $4\times\text{CO}_2\text{HOSING}$ (ca. 8%). In addition, global NPP remains elevated (above the range of variation) for several centuries in all scenarios, with a full return to pre-forcing values not having occurred for $4\times\text{CO}_2$ by the end of the simulation (740 years after the end of the CO_2 increase).

In comparison to CO_2 , the pure effect of additional freshwater hosing only leads to a comparatively small decrease of NPP during AMOC shutdown in the HOSING scenario. Comparing $4\times\text{CO}_2\text{HOSING}$ and $4\times\text{CO}_2$, the freshwater effect is reflected in a weaker deflection of the NPP curve. In other words, the NPP reaches higher minimum and lower maximum values in $4\times\text{CO}_2\text{HOSING}$ and also returns to its initial baseline state earlier. At the exemplarily chosen time of 500 years after the start of the simulation in figure 2 (corresponding to 240 years after the end of forcing), scenario $4\times\text{CO}_2\text{HOSING}$ (figure 2(c)) shows a reduction of the NPP in the NA and an increase in the South Atlantic, in contrast to an increase for the NA and the Indian Ocean for $4\times\text{CO}_2$ (figure 2(a)). Both scenarios $4\times\text{CO}_2$ and $4\times\text{CO}_2\text{HOSING}$ have a distinctive NPP increase in the EEP in common. For $2\times\text{CO}_2$ and $2\times\text{CO}_2\text{HOSING}$ (figures 2(b) and (d)), consistent geographical patterns of a minimal NPP increase are recognizable in the EEP and SO. As can also be seen in figure 1(d), the NPP has almost completely returned to the baseline for these scenarios at $T = 500$. Therefore, we focus on the ‘stronger’ scenarios $4\times\text{CO}_2$ and $4\times\text{CO}_2\text{HOSING}$ in the following sections.

In addition to the global NPP, we will also focus on the SO and the EEP, which are known as HNLC zones. The EEP (figure 1(e)) shows similarities to the global mean values, as the NPP for the $4\times\text{CO}_2$ and $4\times\text{CO}_2\text{HOSING}$ scenarios drops significantly during the forcing phase and afterwards exceeds the baseline (CONTROL) level by far. In comparison, the NPP for the other scenarios swings relatively close to the baseline. For the SO (figure 1(f)), the NPP is strongly influenced by freshwater input in all the HOSING scenarios ($2\times\text{CO}_2\text{HOSING}$, $4\times\text{CO}_2\text{HOSING}$, HOSING), showing a sharp increase at the beginning of the forcing period. After the end of the forcing, this is

followed by a rapid decline in the NPP, especially for $2\times\text{CO}_2\text{HOSING}$ and HOSING, which have already fallen back to the baseline at the end of the forcing at $T = 280$. In contrast, $4\times\text{CO}_2\text{HOSING}$ shows a rather asymptotic decline, similar to $4\times\text{CO}_2$, whereby the NPP moves close to the baseline after $T = 500$.

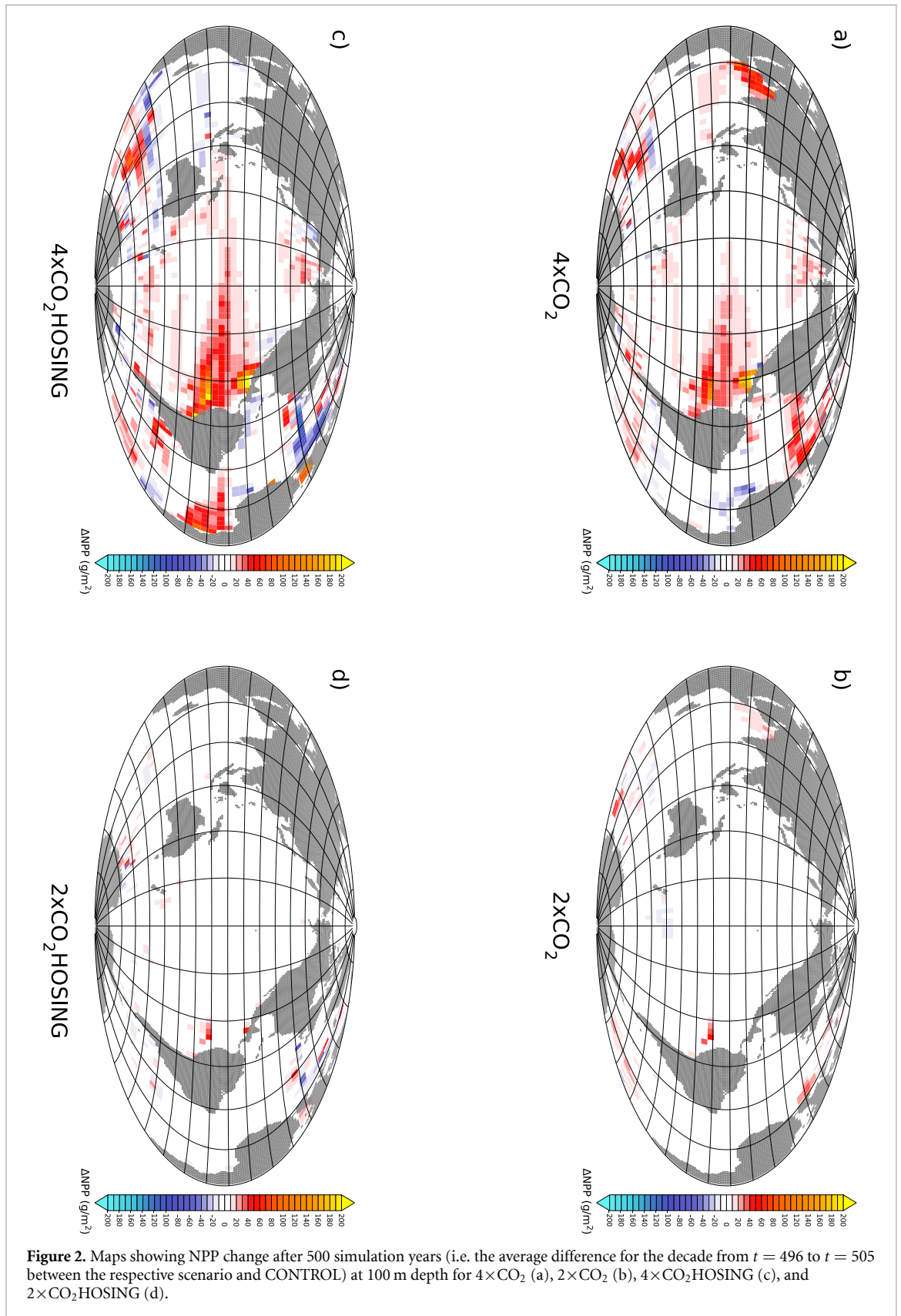
3.3. Long-term change in nutrient limitation

On global average, the limitation of marine NPP by Fe is much more pronounced than by PO_4 , as indicated by significantly lower values of the limiting factor L_{Fe} (see figures 1(e) and (f) over the entire simulation period. Concurrently, Fe availability (i.e. L_{Fe}) increases strongly in the course of the CO_2 elevation for all scenarios, rising to a maximum of +14% for $4\times\text{CO}_2$ and +22% for $4\times\text{CO}_2\text{HOSING}$ shortly after the CO_2 peak is reached. If we compare this with the fact that a moderate L_{Fe} increase of +8% is also observed for the HOSING scenario, it can be deduced that the effects of CO_2 increase and freshwater forcing are essentially additive. As can be seen figure 3(a), L_{Fe} has increased practically worldwide in $4\times\text{CO}_2\text{HOSING}$ and for the majority of the globe in $4\times\text{CO}_2$, especially in the South Atlantic and the equatorial Pacific. This implies that 500 years after the start of the simulation, Fe limitation of NPP in these regions is still reduced over large areas.

In comparison, L_{PO_4} (figures 3(b) and (d)) shows a temporary decrease, which, however, subsides more quickly than L_{Fe} and remains visible only in some places after 500 years. Geographically, this creates a rather mixed picture of decreases and increases, especially in the Atlantic and the Indian Ocean.

3.4. Fe transport

Given that the most plausible explanation for the NPP increase, especially in the EEP, is an increase in Fe availability, a possible transport pathway for Fe into the EEP was traced here. Based on dust input from the Sahara into the NA as a source of iron, figure 4 shows the results of the tracer experiments. In the process, the tracer that was concentrated on the West African coast at $T = 5$ has spread across the entire Atlantic and the Arctic Ocean by $T = 140$. The near-surface concentrations for CONTROL and $4\times\text{CO}_2$ remain very similar until the end of the experiment and show only a moderate increase in the SO apart from the Atlantic. In contrast, there is a much stronger dispersion in $4\times\text{CO}_2\text{HOSING}$, as the area of high tracer concentrations first extends eastward along the SO and then northwards into the Indian Ocean and the EEP. It can be seen in figure 5 that for $4\times\text{CO}_2\text{HOSING}$, different from CONTROL and $4\times\text{CO}_2$, there is no longer any enriched, southward deep water convection in the NA, which results in the near-surface concentration of the tracer.



4. Discussion

Decreasing NPP and nutrient concentrations as a result of the CO_2 increase corresponds to the results that have been found both for socio-economically

based emission scenarios RCP and SSP (Kwiatkowski *et al* 2020, Reygondeau *et al* 2020) as well as idealized scenarios (Boucher *et al* 2012), partly explained by diminishing vertical nutrient supply caused by the increasing stratification of the uppermost water

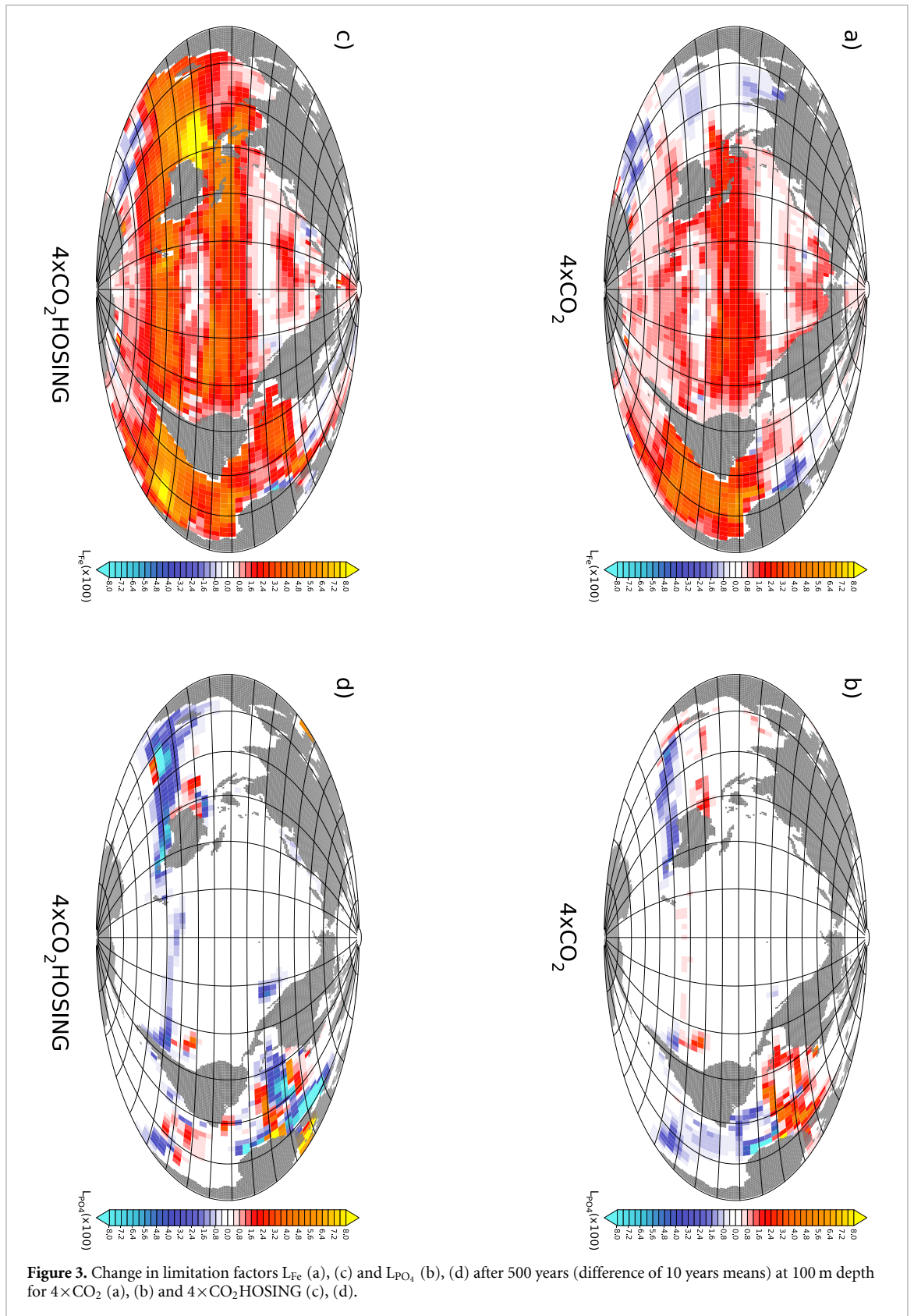
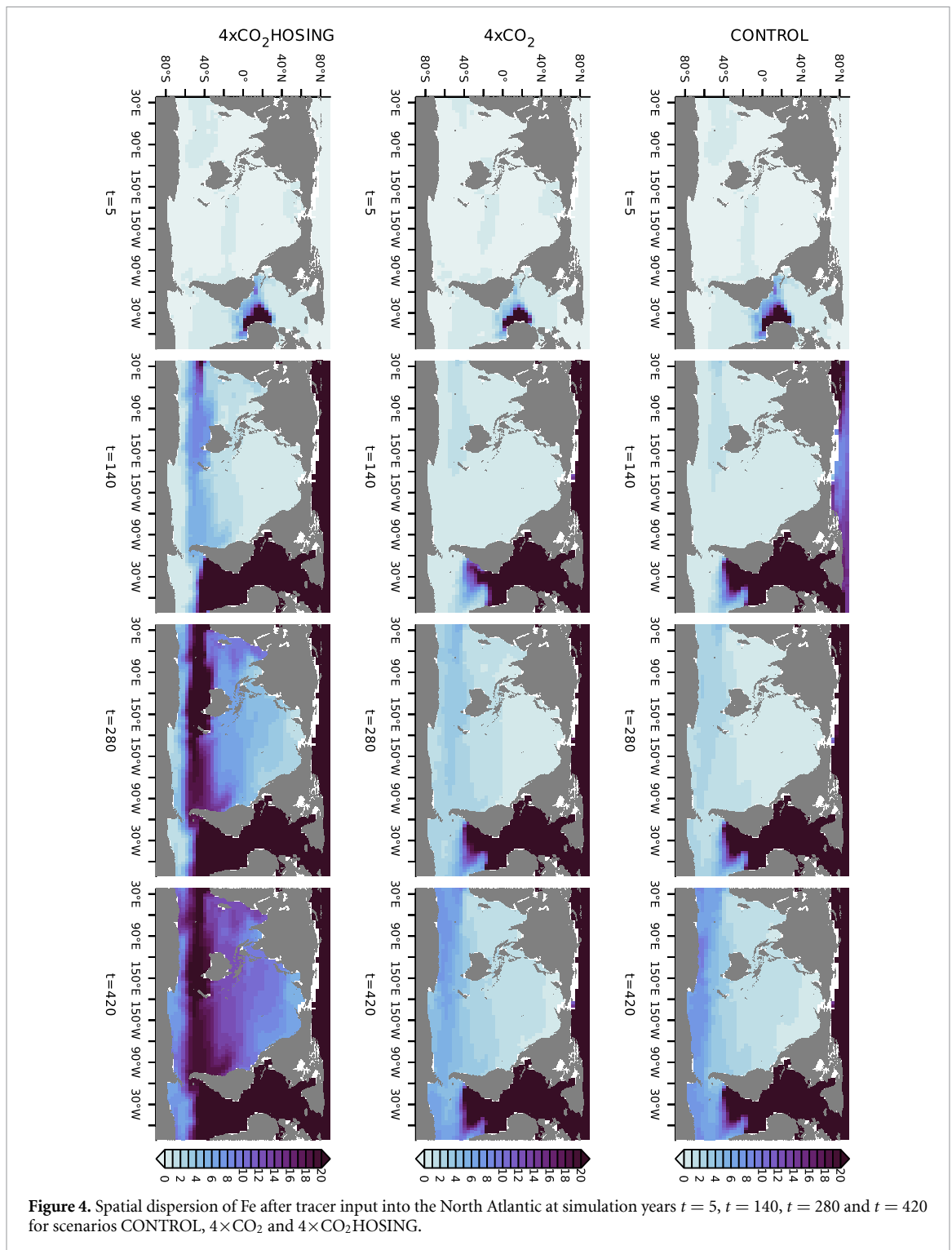


Figure 3. Change in limitation factors L_{Fe} (a), (c) and L_{PO_4} (b), (d) after 500 years (difference of 10 years means) at 100 m depth for $4\times CO_2$ (a), (b) and $4\times CO_2$ HOSING (c), (d).

column under rising temperatures. This largely corresponds to the simulations evaluated here, since in the EEP, SO and Indian Ocean regions, a decrease or increase in mixed layer depth is followed by a similar change in NPP (see figure S2). Apart from this,

however, no overarching temporal coupling can be discerned, whereby geographically the NPP increase coincides with an increase in Fe concentrations in the EEP, the SO and the South Atlantic regions. The EEP can serve here as an exemplary HNLC region, since



the Fe limitation of algal growth there has already been established and an increase in NPP through iron addition has been experimentally proven (IronEx II; Landry *et al* 2000).

Complementary to the vertical mixing already mentioned, the tracer simulations of the $4 \times \text{CO}_2\text{HOSING}$ scenario show that a lateral redistribution of iron from the NA to the EEP is possible. The NA deep water formation usually removes Fe from the near-surface layers, which is regularly brought in by dust from the Sahara (here Saharan

dust being the only external source of marine iron). A possibly extensive weakening of the AMOC due to warming and/or freshwater input would interrupt the removal. This would retain iron in or near the photic zone (see figure 5), which would normally be bound in deep water for many centuries, releasing an increasing amount of Fe over time into the SO and further into the Pacific. If the input is maintained, a long-term NPP increase can develop, provided that there are no other substantial limiting factors. It seems plausible that this could also explain

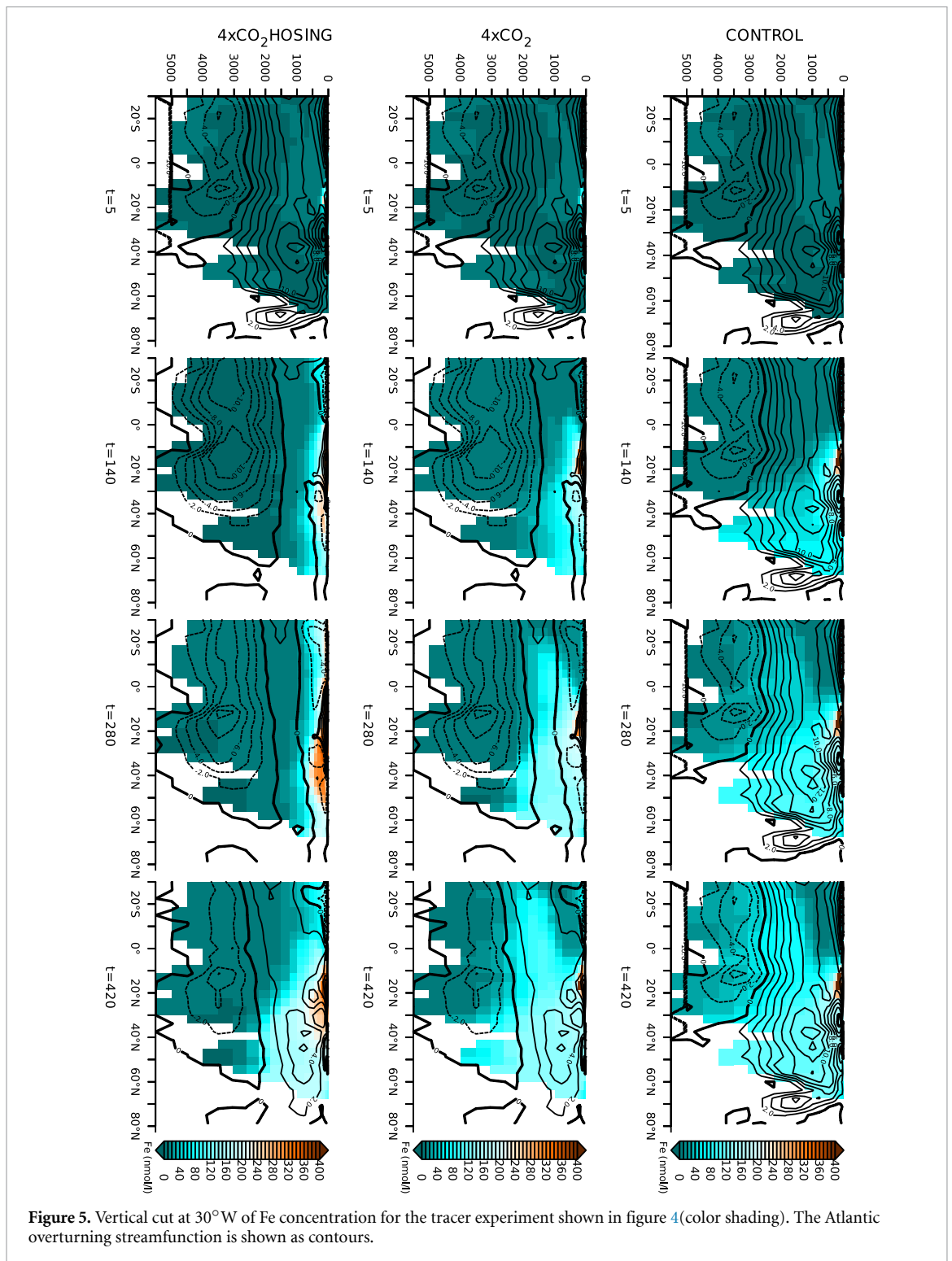


Figure 5. Vertical cut at 30°W of Fe concentration for the tracer experiment shown in figure 4 (color shading). The Atlantic overturning streamfunction is shown as contours.

the increase in NPP in the SO, another Fe-limited HNLC region. The fact that the NPP increase in the SO is significantly lower than in the EEP is probably partly due to a higher phosphate and light limitation, but partly also due to the fact that the SO has a shorter retention time as a “transit station” for iron. In the NA, a sharp decline in PO_4^{3-} appears to be the limiting factor for the NPP, but this does not seem to play a significant role for long-term effects in the

NPP globally due to the generally high availability of phosphate as characterized by L_{PO_4} .

Nevertheless, the mechanism of a lateral redistribution of near-surface iron from the NA appears to necessitate freshwater addition causing a (almost) complete shutdown of the AMOC. The reason is that there is no visible enhancement of tracer concentrations in the same experiment for $4\times\text{CO}_2$ (relative to CONTROL). That means that even a considerable

reduction of the AMOC strength by 60% (as it occurs for $4\times\text{CO}_2$) does not suffice to trigger this event. Considering the AMOC in the context of Greenland meltwater input supports the view of the AMOC as a mediator rather than the initiator of a tipping point cascade (Wunderling *et al* 2021).

Overall, NPP remains increased both globally (figure 1(c)) and in the EEP (figure 2(a)) in the $4\times\text{CO}_2$ scenario, as does the Fe availability L_{Fe} . Preliminary results from another tracer experiment (figure S4) show that surplus iron could be transported from the Arabian Sea (that also receives high loads of dust input from the Sahara). But currently it can only be speculated what could be the cause for iron accumulation in the Arabian Sea (figure S3(a)), especially as there is no increase of Fe availability (figure 3(a)). One possible explanation lies in the enlargement of the oligotrophic (PO_4 poor) region in the Indian Ocean, either by an expansion of Indian subtropical gyre (represented in the model) or due to the intensification of the Indian Monsoon (Katzenberger *et al* 2021, not represented in the model) which may result in a dilution of surface waters by increasing rainfall and river runoff into the Indian Ocean (represented in the model). Thereby, the resulting increase in PO_4 limitation would reduce algal growth (primary production) and the concomitant Fe consumption. The temporary enlargement of the subtropical gyre might also be a relevant factor in the decrease of the global mean of L_{PO_4} , but was not yet further investigated here. If it can be assumed that near-surface transport of iron towards the EEP takes place under $4\times\text{CO}_2$, this would probably be supported by stratification in the Indian Ocean and in the SO (red curves in figure S2).

Another possible source of nutrients for scenarios $2\times\text{CO}_2\text{HOSING}$ and $4\times\text{CO}_2\text{HOSING}$ may also have been created by the mixing from deeper layers in the SO. Comparing HOSING and $4\times\text{CO}_2$ in the SO, it becomes clear how the freshwater input counteracts the stratifying effect of warming (i.e. the CO_2 effect). The massive increase in mixed-layer depth during the forcing phase suggests that if iron is released in the SO, it would also have contributed to the increase in NPP in the EEP. This aspect is all the more important because scenarios $2\times\text{CO}_2\text{HOSING}$ and $4\times\text{CO}_2\text{HOSING}$ may be regarded more realistic than $2\times\text{CO}_2$ and $4\times\text{CO}_2$ as the absence of Greenland melt water input can be assumed to be unlikely in the long term.

In addition to the above-mentioned, possible effects of reduced iron scavenging (i.e. reduced Fe binding to CaCO_3 ballast due to acidification and decalcification) due to increased CaCO_3 decomposition remain to be considered, in our simulations this has turned out to be insignificant for NPP (see figure S1). Grazing by zooplankton can be a significant factor, but due to its complexity it cannot be sufficiently illuminated here. The

associated change in food webs and ecosystems both during and after CO_2 rise (Reygondeau *et al* 2020, Schwinger *et al* 2022) probably needs to be considered in a much more regional, ecological context.

The potential effects of the marine nutrient redistribution presented here are difficult to assess in the long term and will in any case first need to be confirmed. Nevertheless, the consequences for the ecosystems of the EEP alone could be massive, because in addition to all the known consequences of climate change, a century lasting iron fertilization pulse could fundamentally change the food web in the pelagic zone. In terms of societal impacts, this would not only pose a major uncertainty for the global food supply, but also for the structures in the neighboring nations of the affected areas that have grown out of the use of seafood.

5. Conclusion

In this study, data from different idealized model scenarios were analyzed to determine relationships between AMOC strength, NPP, Fe and PO_4 during and after extended periods of atmospheric CO_2 rise and NA freshwater input. Depending on the strength and combination of the applied forcings, a decrease or shutdown of the AMOC is observed. This is accompanied by a transient decrease and post-forcing increase in marine NPP, with a particularly pronounced change in the EEP. Tracer experiments demonstrate that this is due to a global Fe redistribution and fertilization in HNLC areas caused by the AMOC shutdown.

The large-scale redistribution of nutrients, especially Fe, and the accompanying NPP increase can be directly related to the change in ocean currents caused by the collapse of the AMOC. At the same time, similar long-term effects can occur alongside a strong weakening (rather than shutdown) of the AMOC, without a connection between these phenomena being discernible. It remains unclear whether the strength of the AMOC stream function must fall below a critical value to cause an accumulation of near-surface nutrients in the NA, or what mechanisms can trigger this in the Arabian Sea, for example. Due to model limitations, the necessary investigations into climate change-related changes in precipitation, wind flow patterns and the monsoon system cannot be carried out here. Likewise, the tracer simulations applied here can only reflect the passive transport of Fe, but not the biogeochemical changes, for example through scavenging or uptake by phytoplankton. More advanced EMICs or higher resolution Earth system models can help determine whether the effects found here can be reproduced under more realistic conditions. If this proves to be robust, further studies on the impacts on regional marine ecosystems will be necessary.

Data availability statement

All simulation data used here and the scripts used to generate the graphics have been published under Hofmann and Liebermann (2023) (<https://doi.org/10.5880/pik.2023.003>).

Acknowledgment

This project has received funding from the European Union's Horizon 2020 research and innovation programme under Grant Agreement No. 820989 (Project COMFORT, Our common future ocean in the Earth system—quantifying coupled cycles of carbon, oxygen, and nutrients for determining and achieving safe operating spaces with respect to tipping points). The work reflects only the authors' view; the European Commission and their executive agency are not responsible for any use that may be made of the information the work contains. The authors gratefully acknowledge the European Regional Development Fund (ERDF), the German Federal Ministry of Education and Research and the Land Brandenburg for supporting this project by providing resources on the high-performance computer system at the Potsdam Institute for Climate Impact Research. The authors declare no conflict of interest.

ORCID iDs

Ralf Liebermann  <https://orcid.org/0000-0001-5730-0408>

Matthias Hofmann  <https://orcid.org/0000-0001-7259-8396>

Georg Feulner  <https://orcid.org/0000-0001-9215-5517>

References

- Bauer E and Ganopolski A 2010 Aeolian dust modeling over the past four glacial cycles with CLIMBER-2 *Glob. Planet. Change* **74** 49–60
- Behrenfeld M J, Bale A J, Kolber Z S, Aiken J and Falkowski P G 1996 Confirmation of iron limitation of phytoplankton photosynthesis in the equatorial Pacific Ocean *Nature* **383** 508–11
- Boucher O, Halloran P R, Burke E J, Doutriaux-Boucher M, Jones C D, Lowe J, Ringer M A, Robertson E and Wu P 2012 Reversibility in an earth system model in response to CO₂ concentration changes *Environ. Res. Lett.* **7** 024013
- Caesar L, Rahmstorf S, Robinson A, Feulner G and Saba V 2018 Observed fingerprint of a weakening Atlantic Ocean overturning circulation *Nature* **556** 191–6
- Fasham M J R 1993 Modelling the marine biota *The Global Carbon Cycle (Nato ASI Series)* vol I15, ed M Heimann pp 457–504
- Fichefet T and Morales Maqueda M A 1997 Sensitivity of a global sea ice model to the treatment of ice thermodynamics and dynamics *J. Geophys. Res.* **102** 12609–46
- Field C B, Behrenfeld M J, Randerson J T and Falkowski P 1998 Primary production of the biosphere: Integrating Terrestrial and Oceanic Components *Science* **281** 237–40
- Hofer S, Lang C, Amory C, Kittel C, Delhasse A, Tedstone A and Fettweis X 2020 Greater Greenland ice sheet contribution to global sea level rise in CMIP6 *Nat. Commun.* **11** 6289
- Hofmann M and Liebermann R 2023 Climber3 α +C simulations for marine biogeochemistry and primary production *GFZ Data Services* **5** 1107–13
- Hofmann M, Mathesius S, Kriegler E, van Vuuren D P and Schellnhuber H J 2019 Strong time dependence of ocean acidification mitigation by atmospheric carbon dioxide removal *Nat. Commun.* **10** 5592
- Hofmann M and Morales Maqueda M A 2011 The response of Southern Ocean eddies to increased midlatitude westerlies: a non-eddy resolving model study *Geophys. Res. Lett.* **38** L03605
- Hofmann M and Morales Maqueda M A 2006 Performance of a second-order moments advection scheme in an Ocean General Circulation Model *J. Geophys. Res.* **111** C05006
- Hofmann M and Schellnhuber H-J 2009 Oceanic acidification affects marine carbon pump and triggers extended marine oxygen holes *Proc. Natl. Acad. Sci. USA* **106** 3017–22
- Jeltsch-Thoemmes A, Stocker T F and Joos F 2020 Hysteresis of the earth system under positive and negative CO₂ emissions *Environ. Res. Lett.* **15** 124026
- Katzenberger A, Schewe J, Pongratz J and Levermann A 2021 Robust increase of Indian monsoon rainfall and its variability under future warming in CMIP6 models *Earth Syst. Dyn.* **12** 367–86
- Kolber Z S, Barber R T, Coale K H, Fitzwater S E, Greene R M, Johnson K S, Lindley S and Falkowski P G 1994 Iron limitation of phytoplankton photosynthesis in the equatorial Pacific Ocean *Nature* **371** 145–9
- Kwiatkowski L et al 2020 Twenty-first century ocean warming, acidification, deoxygenation and upper-ocean nutrient and primary production decline from CMIP6 model projections *Biogeosciences* **17** 3439–70
- Landry M R, Ondrusek M E, Tanner S J, Brown S L, Constantinou J, Bidigare R R, Coale K H and Fitzwater S 2000 Biological response to iron fertilization in the eastern equatorial Pacific (IronEx II). I. Microplankton community abundances and biomass *Mar. Ecol. Prog. Ser.* **201** 27–42
- Lenton T M, Held H, Kriegler E, Hall J W, Lucht W, Rahmstorf S and Schellnhuber H J 2008 Tipping elements in the Earth's climate system *Proc. Natl. Acad. Sci. USA* **105** 1786–93
- Liu W, Xie S P, Liu Z and Zhu J 2017 Overlooked possibility of a collapsed Atlantic meridional overturning circulation in warming climate *Sci. Adv.* **3** e1601666
- Longhurst A, Sathyendranath S, Platt T and Caverhill C 1995 An estimate of global primary production in the ocean from satellite radiometer data *J. Plankton Res.* **17** 1245–71
- Martin J H and Fitzwater S E 1988 Iron deficiency limits phytoplankton growth in the north-east Pacific subarctic *Nature* **331** 341–43
- Mathesius S, Hofmann M, Caldeira K and Schellnhuber H J 2015 Long-term response of oceans to CO₂ removal from the atmosphere *Nat. Clim. Change* **5** 1107–13
- Meinshausen M, Raper S C B and Wigley T M L 2011 Emulating coupled atmosphere-ocean and carbon cycle models with a simpler model, MAGICC6 – Part 1: model description and calibration *Atmos. Chem. Phys.* **11** 1417–56
- Montoya M, Griesel A, Levermann A, Mignot J, Hofmann M, Ganopolski A and Rahmstorf S 2005 The earth system model of intermediate complexity CLIMBER-3 α . Part I: description and performance for present-day conditions *Clim. Dyn.* **25** 237–63
- Pacanowski R C and Griffies S M 1999 The MOM-3 manual, *Technical Report 4*, NOAA/Geophysical Fluid Dynamics Laboratory (available at: https://mom-ocean.github.io/assets/pdfs/MOM3_manual.pdf)
- Parekh P, Follows M J and Boyle E A 2005 Decoupling of iron and phosphate in the global ocean *Glob. Biogeochem. Cycles* **19** GB2020

- Petoukhov V, Ganopolski A, Brovkin V, Claussen M, Eliseev A, Kubatzki C and Rahmstorf S 2000 CLIMBER-2: a climate system model of intermediate complexity. Part I: model description and performance for present climate *Clim. Dyn.* **16** 1–17
- Rahmstorf S 1995 Bifurcations of the Atlantic thermohaline circulation in response to changes in the hydrological cycle *Nature* **378** 145–49
- Reygondeau G, Cheung W W L, Wabnitz C C C, Lam V W Y, Froelicher T and Maury O 2020 Climate change-induced emergence of novel biogeochemical provinces *Front. Mar. Sci.* **7** 657
- Reygondeau G, Longhurst A, Martinez E, Beaugrand G and Maury D O 2013 Dynamic biogeochemical provinces in the global ocean *Glob. Biogeochem. Cycles* **27** 1046–58
- Rousseaux C S and Gregg W W 2014 Interannual variation in phytoplankton primary production at a global scale *Remote Sens.* **6** 1–19
- Schwinger J, Asaadi A, Goris N and Lee H 2022 Possibility for strong northern hemisphere high-latitude cooling under negative emissions *Nat. Commun.* **13** 1095
- S  f  rian R *et al* 2020 Tracking improvement in simulated marine biogeochemistry between CMIP5 and CMIP6 *Curr. Clim. Change Rep.* **6** 166–177
- Six K D and Maier-Reimer E 1996 Effects of plankton dynamics on seasonal carbon fluxes in an ocean general circulation model *Glob. Biogeochem. Cycles* **10** 559–83
- Steffen W *et al* 2021 Trajectories of the earth system in the anthropocene *Proc. Natl Acad. Sci. USA* **115** 8252–59
- Sunda W G and Huntsman S A 1997 Interrelated influence of iron, light and cell size on marine phytoplankton growth *Nature* **390** 389–92
- Vichi M, Allen J I, Masina S and Hardman Mountford N J 2011 The emergence of ocean biogeochemical provinces: a quantitative assessment and a diagnostic for model evaluation *Glob. Biogeochem. Cycles* **25**
- Weijer W, Cheng W, Garuba O A, Hu A and Nadiga B T 2020 CMIP6 models predict significant 21st century decline of the Atlantic meridional overturning circulation *Geophys. Res. Lett.* **47** 1–14
- Wunderling N, Donges J F, Kurths J and Winkelmann R 2021 Interacting tipping elements increase risk of climate domino effects under global warming *Earth Sys. Dyn.* **12** 601–19